

# Laser Power Dependence of Mass Spectral Signatures from Individual Bacterial Spores in Bioaerosol Mass Spectrometry

Paul T. Steele,<sup>†,‡</sup> Herbert J. Tobias,<sup>†</sup> David P. Fergenson,<sup>†</sup> Maurice E. Pitesky,<sup>†</sup> Joanne M. Horn,<sup>†</sup> Gregg A. Czerwiec,<sup>†,§</sup> Scott C. Russell,<sup>†,§</sup> Carlito B. Lebrilla,<sup>§</sup> Eric E. Gard,<sup>†</sup> and Matthias Frank<sup>\*,†</sup>

Lawrence Livermore National Laboratory, 7000 East Avenue, L-174, Livermore, California 94550, and Department of Applied Science and Department of Chemistry, University of California at Davis, 1 Shields Avenue, Davis, California 95616

**Bioaerosol mass spectrometry is being developed to analyze and identify biological aerosols in real time. Characteristic mass spectra from individual bacterial endospores of *Bacillus subtilis* var. *niger* were obtained in a bipolar aerosol time-of-flight mass spectrometer using a pulsed 266-nm laser for molecular desorption and ionization. Spectra from single spores collected at an average fluence of  $\sim 0.1$  J/cm<sup>2</sup> frequently contain prominent peaks attributed to arginine, dipicolinic acid, and glutamic acid, but the shot-to-shot (spore-to-spore) variability in the data may make it difficult to consistently distinguish closely related *Bacillus* species with an automated routine. Fortunately, a study of the laser power dependence of the mass spectra reveals clear trends and a finite number of “spectral types” that span most of the variability. This, we will show, indicates that a significant fraction of the variability must be attributed to fluence variations in the profile of the laser beam.**

Single-particle aerosol mass spectrometry has become an established technique for the rapid chemical analysis of individual aerosol particles.<sup>1</sup> The technique has been developed and implemented in forms such as RSMS,<sup>2</sup> PALMS,<sup>3</sup> LAMPAS,<sup>4,5</sup> RTAMS,<sup>6</sup> and ATOFMS,<sup>7</sup> which we helped to develop. In typical systems, aerosol particles are sampled directly from the atmosphere into the vacuum system of a mass spectrometer.<sup>8</sup> As particles approach the ion source region, they cross and scatter light from one or two CW laser beams.<sup>9</sup> The scattered light indicates the particle

size, speed, and location. This information is then used to trigger one or two high-intensity pulsed lasers that desorb and ionize molecules from the particles. The full spectrum of ions can then be measured, at once, in systems using a time-of-flight mass spectrometer. Because these single-particle mass spectrometers characterize individual airborne particles in a fraction of a second without reagents or sample preparation, they have great potential as rapid airborne biological threat detectors even in environments with high concentrations of background particles.

In such an application, it is necessary to identify particles on the basis of single mass spectra without the benefits of averaging to obtain greater consistency or better signal-to-noise ratios. Clearly this means that the information content in every spectrum must be maximized. Furthermore, sources of variability in the spectra should be identified, quantified, and minimized. Data analysis procedures and classification algorithms must be efficient and capable of dealing with any remaining shot-to-shot variation. All of this must be done without compromising the rate at which spectra can be acquired and analyzed. Several of us were involved in the previous development of ATOFMS.<sup>7,10</sup> We have, therefore, begun to modify and tailor this technology for the rapid detection and identification of biological aerosols. To prove and develop the technique of bioaerosol mass spectrometry (BAMS), we are currently using a combination of modified commercial ATOFMS instrumentation and our own real-time data analysis software. To achieve greatly improved performance, we are presently designing and building a new generation of BAMS hardware.

Here we present our first results from an investigation of the dependence of single bacterial endospore mass signatures on desorption/ionization laser pulse energy and fluence. Our measurements were performed on spores aerosolized directly from water without the addition of a chemical matrix. While MALDI-type measurements have been performed on ensembles of biological particles<sup>11–13</sup> and new techniques have been developed to coat single aerosol particles “on-the-fly” with a matrix,<sup>14–16</sup> we are exploring matrix-free desorption/ionization because liquid

\* Corresponding author. E-mail: frank1@llnl.gov. Telephone: 925-423-5068. Fax: 925-424-2778.

<sup>†</sup> Lawrence Livermore National Laboratory.

<sup>‡</sup> Department of Applied Science, University of California at Davis.

<sup>§</sup> Department of Chemistry, University of California at Davis.

- (1) Suess, D. T.; Prather, K. A. *Chem. Rev.* **1999**, *99*, 3007–3035.
- (2) Johnston, M. V.; Wexler, A. S. *Anal. Chem.* **1995**, *67*, A721–A726.
- (3) Murphy, D. M.; Thomson, D. S. *Aerosol Sci. Technol.* **1995**, *22*, 237–249.
- (4) Hinz, K. P.; Kaufmann, R.; Spengler, B. *Anal. Chem.* **1994**, *66*, 2071–2076.
- (5) Hinz, K. P.; Kaufmann, R.; Spengler, B. *Aerosol Sci. Technol.* **1996**, *24*, 233–242.
- (6) Lazar, A.; Reilly, P. T. A.; Whitten, W. B.; Ramsey, J. M. *Environ. Sci. Technol.* **1999**, *33*, 3993–4001.
- (7) Gard, E.; Mayer, J. E.; Morrical, B. D.; Dienes, T.; Fergenson, D. P.; Prather, K. A. *Anal. Chem.* **1997**, *69*, 4083–4091.
- (8) Mallina, R. V.; Wexler, A. S.; Johnston, M. V. *J. Aerosol. Sci.* **1999**, *30*, 719–738.
- (9) Salt, K.; Noble, C. A.; Prather, K. A. *Anal. Chem.* **1996**, *68*, 230–234.

(10) Song, X. H.; Hopke, P. K.; Fergenson, D. P.; Prather, K. A. *Anal. Chem.* **1999**, *71*, 860–865.

(11) Fenselau, C.; Demirev, P. A. *Mass Spectrom. Rev.* **2001**, *20*, 157–171.

(12) Van Baar, B. L. M. *Fems Microbiol. Rev.* **2000**, *24*, 193–219.

(13) Lay, J. O. *Mass Spectrom. Rev.* **2001**, *20*, 172–194.

(14) He, L.; Murray, K. K. *J. Mass Spectrom.* **1999**, *34*, 909–914.

(15) Jackson, S. N.; Murray, K. K. *Anal. Chem.* **2002**, *74*, 4841–4844.

consumables may be undesirable in a fully autonomous biode-tection system. With or without matrix, the laser pulse used to desorb and ionize molecules from aerosol particles is, arguably, one of the most important variables in BAMS. It is widely known that MALDI ion velocities and ion yields are fluence dependent.<sup>17–19</sup> Furthermore, spectra from single nonbiological particles have been observed to change dramatically with laser energy.<sup>3,20</sup> Other groups have used single-particle mass spectrometers to look at biological particles,<sup>21–24</sup> but the studies presented here are, to our knowledge, the first attempt to systematically correlate single-particle mass spectra from bacterial spores with laser energy and beam profile measurements. Furthermore, we believe that we are the first to present both positive and negative ion mass spectra collected from the same individual spore. All of the measurements presented here were performed on spores of a single species, *Bacillus subtilis var. niger* (formerly *Bacillus globigii* and recently renamed *Bacillus atrophaeus*), but preliminary experiments with other *Bacillus* species show similar types of laser power dependence. The comparison of mass signatures from various species and other biological and nonbiological aerosols will be presented in a separate publication.<sup>25</sup>

## EXPERIMENTAL SECTION

The system utilized for this study consists of two basic components: a commercial single-particle mass spectrometer (TSI model 3800) and a data analysis software package developed by the authors. In the laboratory setting, separate equipment generates an artificial aerosol for experiments. The overall instrumental layout is shown in Figure 1. Spores are aerosolized from aqueous solution, dried, and sampled into the single-particle mass spectrometer, ultimately producing mass spectra that are saved to disk. The saved data can be retrieved for instant analysis and on-line identification or stored and accumulated for later analysis off-line, as was done for this paper.

**Spore Preparation.** *B. subtilis var. niger* (ATCC 9372, Dugway Proving Ground, Dugway, UT) cells were grown to mid-log phase in 1/4×TY media and then aliquoted in a 1:25 dilution into 75 mL of 1/4×TY media. The *Bacillus* sporulated in 1/4×TY sporulation media in a shaker incubator at 32 °C until ~90% of all the cells were refractile (3–4 days). Phase contrast microscopy

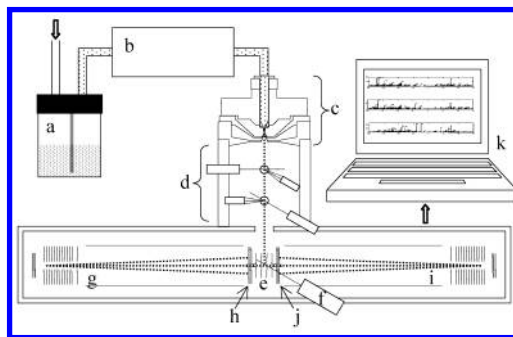


Figure 1. Schematic diagram of the laboratory setup used to obtain dual-polarity mass spectra from individual *B. subtilis var. niger* spores. Dry air passes through a Collision nebulizer (a) producing an aerosol of spore-containing water droplets. The water is removed with a drier (b), and the spores are directed into the mass spectrometer inlet (c). The spores pass through the sizing region (d) and arrive at the center of the ion source region (e). A frequency-quadrupled, Q-switched Nd:YAG laser (f) then desorbs and ionizes molecules from the spores. Positive ions (g) are accelerated and then reflected toward a set of microchannel plates (h). Negative ions (i) are accelerated in the opposite direction and detected with a separate set of microchannel plates (j). The digitized MCP signals are then stored and analyzed on a computer (k).

and spore staining were used to confirm the presence of bacterial spores. Gram stains were used in order to identify vegetative cells and nonrefractile cells that were still developing into spores. Spores were harvested by centrifugation at 8000g for 12 min and washed in cold double-distilled water. After being washed three times, the spores were reconstituted in double-distilled-water at concentrations of ~10<sup>6</sup> spores/mL as determined using a Petroff-Hauser counting chamber. To confirm the purity of the cultures, an aliquot from each culture was collected and a 500-base pair region of the 16s rDNA was sequenced (MIDI Labs, Newark, DE).

**Aerosol Generation.** The spore solution was aerosolized using a Collision nebulizer<sup>26,27</sup> with a ~2.5 L/min flow of clean, dry air. The wet bioaerosol was dried with a diffusion drier containing activated silica gel desiccant and was then piped through copper tubing to the aerosol mass spectrometer inlet. The mean aerodynamic diameter of the aerosol particles at the inlet was determined by aerodynamic sizing (see below) to be 0.92 μm, which is consistent with the value expected for single spores. (The aerodynamic diameter of a particle is equivalent to the diameter of a unit density sphere with the same settling velocity.) Eighty percent of the particles had a diameter within ±0.05 μm of the mean, but occasionally much larger diameters (2–3 μm) were observed. These most likely represent clusters of two or more spores. Approximately 1 in 10 particles had a smaller diameter, but few of these are believed to represent intact spores.

**Aerosol Time-of-Flight Mass Spectrometer.** A detailed description of a similar single-particle mass spectrometer already exists in the literature,<sup>7</sup> but a brief description will be given here for clarity. The spectrometer draws air and entrained aerosol particles from the environment (or from the output of a nebulizer connected to the instrument by a copper tube) through a converging nozzle into vacuum at a rate of ~1 L/min. The

- (16) Stowers, M. A.; van Wuijckhuijse, A. L.; Marijnissen, J. C. M.; Scarlett, B.; van Baar, B. L. M.; Kientz, C. E. *Rapid Commun. Mass Spectrom.* **2000**, *14*, 829–833.
- (17) Feldhaus, D.; Menzel, C.; Berkenkamp, S.; Hillenkamp, F.; Dreisewerd, K. *J. Mass Spectrom.* **2000**, *35*, 1320–1328.
- (18) Berkenkamp, S.; Menzel, C.; Hillenkamp, F.; Dreisewerd, K. *J. Am. Soc. Mass Spectrom.* **2002**, *13*, 209–220.
- (19) Westmacott, G.; Ens, W.; Hillenkamp, F.; Dreisewerd, K.; Schurenberg, M. *Int. J. Mass Spectrom.* **2002**, *221*, 67–81.
- (20) Noble, C. A.; Prather, K. A. *Aerosol Sci. Technol.* **1998**, *29*, 294–306.
- (21) Sinha, M. P.; Platz, R. M.; Vilker, V. L.; Friedlander, S. K. *Int. J. Mass Spectrom. Ion Process.* **1984**, *57*, 125–133.
- (22) Sinha, M. P.; Platz, R. M.; Friedlander, S. K.; Vilker, V. L. *Appl. Environ. Microbiol.* **1985**, *49*, 1366–1373.
- (23) Gieray, R. A.; Reilly, P. T. A.; Yang, M.; Whitten, W. B.; Ramsey, J. M. *J. Microbiol. Methods* **1997**, *29*, 191–199.
- (24) Parker, E. P.; Trahan, M. W.; Wagner, J. S.; Rosenthal, S. E.; Whitten, W. B.; Gieray, R. A.; Reilly, P. T. A.; Lazar, A. C.; Ramsey, J. M. *Field Anal. Chem. Technol.* **2000**, *4*, 31–42.
- (25) Fergenson, D. P.; Pitesky, M. E.; Tobias, H. J.; Steele, P. T.; Czerwieńiec, G. A.; Russell, S. C.; Lebrilla, C. B.; Horn, J. M.; Coffee, K. R.; Srivastava, A.; Pillai, S. P.; Shih, M.-T. P.; Hall, H. L.; Ramponi, A. J.; Chang, J. T.; Langlois, R. G.; Estacio, P. L.; Hadley, R. T.; Frank, M.; Gard, E. E. Submitted for publication.

(26) May, K. R. *J. Aerosol. Sci.* **1973**, *4*, 235–243.

(27) Kinney, P. D.; Pui, D. Y. H.; Mulholland, G. W.; Bryner, N. P. *J. Res. Natl. Inst. Stand. Technol.* **1991**, *96*, 147–176.

supersonic expansion from the nozzle focuses the aerosol particles into a vertical beam that passes downward through three stages of differential pumping, through a sizing region, and finally into an ion source region at the center of a dual-polarity mass spectrometer. This process imparts each particle with a velocity dependent on its aerodynamic diameter. An aerosol particle that has been properly focused and accelerated crosses two 532-nm CW laser beams in the sizing region (at  $\sim 10^{-4}$  Torr) causing two bursts of scattered light that are detected by photomultiplier tubes. The time delay between these bursts is used to determine the particle's velocity and, with proper calibration, its aerodynamic diameter.<sup>28</sup> Once the particle's position and velocity are known, the system predicts when the particle will reach the ion source region (at  $\sim 10^{-7}$  Torr) and triggers the desorption/ionization (D/I) laser accordingly. A single pulse from the D/I laser both desorbs and ionizes molecules from the aerosol particle. The ionized molecules are then extracted into two opposing reflectron time-of-flight mass spectrometers whose outputs can be combined to produce a final mass spectrum with both positive and negative ion peaks. In both polarities, a two-stage, static extraction potential is used such that singly charged ions are imparted with  $\sim 6.4$  keV of energy over a 1-cm path. The mass spectrum, laser pulse energy, particle size, and several other parameters are then saved to disk where they can be retrieved for automated real-time identification or stored for later analysis.<sup>10,29,30</sup>

It should be pointed out that the commercial instrument was not designed for use as a sensitive biodetector. Preliminary experiments indicate that only  $\sim 5$  particles are tracked for every 2000 particles drawn into the spectrometer. Only one of these tracked particles is then hit by the D/I laser, producing a spectrum. The maximum rate at which spectra can be acquired, regardless of the aerosol particle concentration, is on the order of 2 Hz due to instrumental limitations. Significant improvements are needed for a practical biodetector, which is why we are presently building a new, far more advanced system for BAMS.

**Desorption/Ionization Laser.** The D/I laser utilized for the measurements reported here is a Q-switched, frequency-quadrupled Nd:YAG laser (Ultra CFR, Big Sky Laser Technologies, Inc.) emitting pulses with a wavelength of 266 nm, a pulse length of less than 6 ns, and a roughly Gaussian beam profile (unaltered, as received by the supplier). The wavelength is nearly coincident with an absorption peak in dipicolinic acid (DPA),<sup>31</sup> which is known to constitute a significant fraction of a *Bacillus* spore's mass. The laser pulse energies used ranged from 0.2 to 1.0 mJ and were obtained by adjusting the flash lamp power (which is not optimal for producing consistent laser profiles). The beam was brought to a focus, in vacuum, before the target region and allowed to expand until it was  $\sim 400$   $\mu\text{m}$  in diameter (fwhm) at the target plane (the plane perpendicular to the laser beam where particles are most likely to be hit).

Terms describing laser energy, power, fluence, and intensity are often used loosely in practice so it is worthwhile to clarify

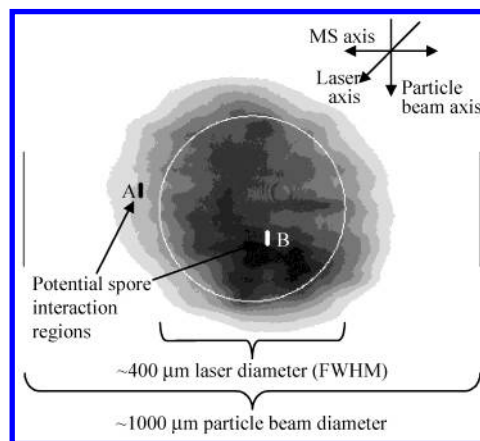


Figure 2. Profile of a single laser pulse with two examples of regions (A and B) in which spores could interact with the pulse. The dimensions of the regions have been magnified by a factor of 10 (area  $\times 100$ ). The width of the focused particle stream is roughly 1 mm, as indicated by the vertical lines, so successive spores will interact with different regions of the laser pulse and absorb different amounts of energy even if the pulse energy is fixed. The different interaction regions also result in slightly different ion flight times since there is a large, static electric field in the ion source region. The area enclosed by the large circle is equal to the area in the profile where the fluence is greater than or equal to half of the maximum fluence.

their meaning here. We use intensity (measured in  $\text{W}/\text{cm}^2$  or  $\text{W}/\mu\text{m}^2$ ) to describe the rate at which energy is incident on an area (the strict definition is power per solid angle). Fluence (in  $\text{J}/\text{cm}^2$  or  $\text{nJ}/\mu\text{m}^2$ ) describes the net energy incident on an area and, in our case, is equivalent to the "intensity" integrated over the temporal duration of the 6 ns laser pulse. The total pulse energy (in J or mJ) is the fluence integrated over the spatial cross section of the laser beam.

The total pulse energy can be recorded for every analyzed particle, as was done here, but this quantity has limited value. The area over which the laser profile has an intensity greater than or equal to half its peak intensity is  $\sim 1.3 \times 10^5$   $\mu\text{m}^2$ . The cross-sectional area of a spore is less than 1  $\mu\text{m}^2$ . Over the course of a 6-ns laser pulse the spore does move slightly, but even a spore traveling at 400 m/s traverses only 2.4  $\mu\text{m}$  and samples a very small fraction of the laser pulse. It is, therefore, the *local* intensity and *local* fluence that determine the maximum energy a spore may absorb.

Figure 2 contains an image of our laser's profile that is clearly not uniform in fluence or intensity. This is significant because preliminary experiments indicate that the focused stream of aerosol particles is more than 1 mm wide at the point where it intersects the laser. The result of this is that successive aerosol particles interact with different portions of the laser beam and absorb different amounts of energy even if the pulse energy is fixed. A spore located near region B in Figure 2, for example, would encounter higher fluences and absorb more energy than an identical spore located near region A. Unfortunately, we have no means of determining precisely where a given particle interacts with the laser pulse and cannot, therefore, determine the local fluence that a particle encounters or how much energy a given particle absorbs. Nonetheless, we can control and measure the average fluence (i.e., the pulse energy) and use statistical arguments to infer the fluence dependence.

(28) Noble, C. A.; Prather, K. A. *Environ. Sci. Technol.* **1996**, *30*, 2667–2680.

(29) Fergenson, D. P.; Liu, D. Y.; Silva, P. J.; Prather, K. A. *Chemom. Intell. Lab. Syst.* **1997**, *37*, 197–203.

(30) Fergenson, D. P.; Song, X. H.; Ramadan, Z.; Allen, J. O.; Hughes, L. S.; Cass, G. R.; Hopke, P. K.; Prather, K. A. *Anal. Chem.* **2001**, *73*, 3535–3541.

(31) Nudelman, R.; Bronk, B. V.; Efrima, S. *Appl. Spectrosc.* **2000**, *54*, 445–449.

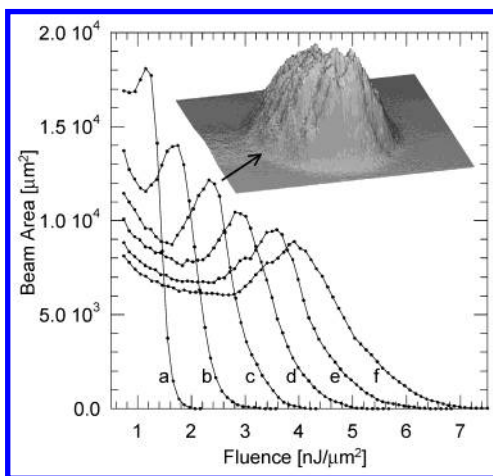


Figure 3. Laser fluence distributions produced by the six laser energy settings used. Distributions correspond to average laser pulse energies of 0.21 (a), 0.34 (b), 0.50 (c), 0.66 (d), 0.84 (e), and 1.02 mJ (f), respectively. A broad range of fluences is present in all laser pulses. This is expected to cause variability in the patterns of ions produced by the D/I laser from shot to shot. The inset shows a typical 0.5 mJ, 266-nm D/I laser pulse profile (single shot). The diameter of the profile is  $\sim 400 \mu\text{m}$  (fwhm).

Figure 3 shows fluence distributions for the six laser settings used (0.21, 0.34, 0.50, 0.66, 0.84, and 1.02 mJ average pulse energies) and a different view of the profile shown in Figure 2. The units of  $\text{nJ}/\mu\text{m}^2$  ( $1 \text{ nJ}/\mu\text{m}^2 = 0.1 \text{ J}/\text{cm}^2$ ) are convenient since the physical cross section of a spore is on the order of  $1 \mu\text{m}^2$ . The distributions in Figure 3 are useful, but not commonly presented, so a short description of their generation and significance is in order. For each of the six laser settings, multiple images of the laser beam cross section slightly in front of, at, and slightly behind the target plane were acquired with a Coherent LaserCam IIID camera. For each image, the absolute fluence was calculated for each pixel and a histogram of the values was produced. The number of pixels falling in each fluence bin was multiplied by the area per pixel ( $\sim 10.7 \mu\text{m}^2$ ) to find the total area represented by the bin in the laser cross section. Histograms from the 49 images collected at each laser setting were then combined with a weighted average to produce the results in Figure 3. The curves show the range of fluences that an individual aerosol particle may encounter. If we make the simplifying assumption that the aerosol particle distribution is uniform across the laser pulse (recall that the particle beam diameter is much larger than the laser beam diameter), the area in the beam at a given fluence should be roughly proportional to the probability of a spore interacting with that fluence. By including data from multiple laser shots and three spatial planes, the effects of shot-to-shot energy and profile variations are reflected in the curves for particles whose positions may vary in all three spatial dimensions.

As expected for our roughly Gaussian laser profile, we observe a broad distribution of fluences for all the laser settings used. At the highest setting, the fluence ranges from zero to more than  $7 \text{ nJ}/\mu\text{m}^2$ . The broad distributions result primarily from the laser profile, but pulse-to-pulse energy variations also contribute. The distribution of laser pulse energies (measured while actively collecting spectra at a fixed laser energy setting) is roughly Gaussian with a standard deviation of 14% at the lowest setting, which shrinks to 4% at the highest. Ignoring profile variations for

the moment, these pulse energy variations could cause the fluence to vary from its mean value by  $\pm 14\%$ . The profile, however, causes the fluence to range from zero to perhaps several times the mean. Any effects due to shot-to-shot pulse energy variations (at fixed laser setting) will be smaller than those due to the laser profile.

A potential source of error in the calculated fluence values is the camera system and associated optics. Inhomogeneities in the CCD response have not yet been fully quantified. Furthermore, the system produces images of a particular plane in space, but it is very difficult to ensure that this plane is exactly coincident with the center of the aerosol particle stream (i.e., the target plane). We estimate that our focusing error may be 1–2 mm; therefore, the errors in the calculated fluences may be 5–10%.

**Data Collection and Calibration.** With the experimental setup described, 1000 dual-polarity mass spectra from single *B. subtilis var. niger* spores were collected at each of the six laser settings mentioned earlier. The data were collected without modification of the single-particle mass spectrometer or associated laser systems, so the range and particular values of the average laser energy were limited. (We have since added external optics to allow for continuous adjustment of the laser energy throughout the desired range at fixed flashlamp pump energy.) Laser settings below 0.2 mJ did not produce spectra at a practical rate. Furthermore, the majority of the spectra that were produced had very few ion peaks, which made them difficult to calibrate accurately and ill-suited for identification purposes. Energies above  $\sim 1.0$  mJ did not produce significant spectral changes compared to spectra taken at 1.0 mJ except for increasing fragmentation.

The raw spectral data consist of digitized ion signals from the microchannel plate detectors recorded at 2-ns time intervals (for both the positive and negative ions). Various factors introduce a small, but noticeable jitter into the calibration of the mass spectrometer. The majority of this jitter is attributed to the  $\sim 400\text{-}\mu\text{m}$  diameter of the region in which aerosol particles may be hit by the D/I laser (Figure 2) and the voltage gradient across this region. The laser could be focused more tightly, but this would decrease the likelihood that a tracked aerosol particle would be hit by the laser pulse. To deal with the jitter, a rough calibration of each set of data was obtained manually and then subsequently refined for each individual spectrum with an automated routine that we developed.

## RESULTS AND DISCUSSION

Figure 4 shows individual dual-polarity mass spectra obtained from single spores at three (of the six) D/I laser energy settings. In producing each of the “full” spectra in Figure 4, the “half” spectrum from positive ions and the “half” spectrum from negative ions were first calibrated separately and then linked together. Joining the polarities together stresses the point that both positive and negative ions are measured simultaneously for each particle and should be considered in unison. Negative ions have negative mass-to-charge ratios ( $m/q < 0$ ) and positive ions have positive mass-to-charge ratios (i.e., the “charge” or “ $q$ ” is the actual net charge on the ion and not just the magnitude). There are separate microchannel plate detectors for the positive and negative ions, and thus, the vertical scaling (gain) may be somewhat different for the two halves of each spectrum. Nonetheless, the scales are consistent from spectrum to spectrum in all of the figures (i.e., if two positive peaks or two negative peaks have the same area, they

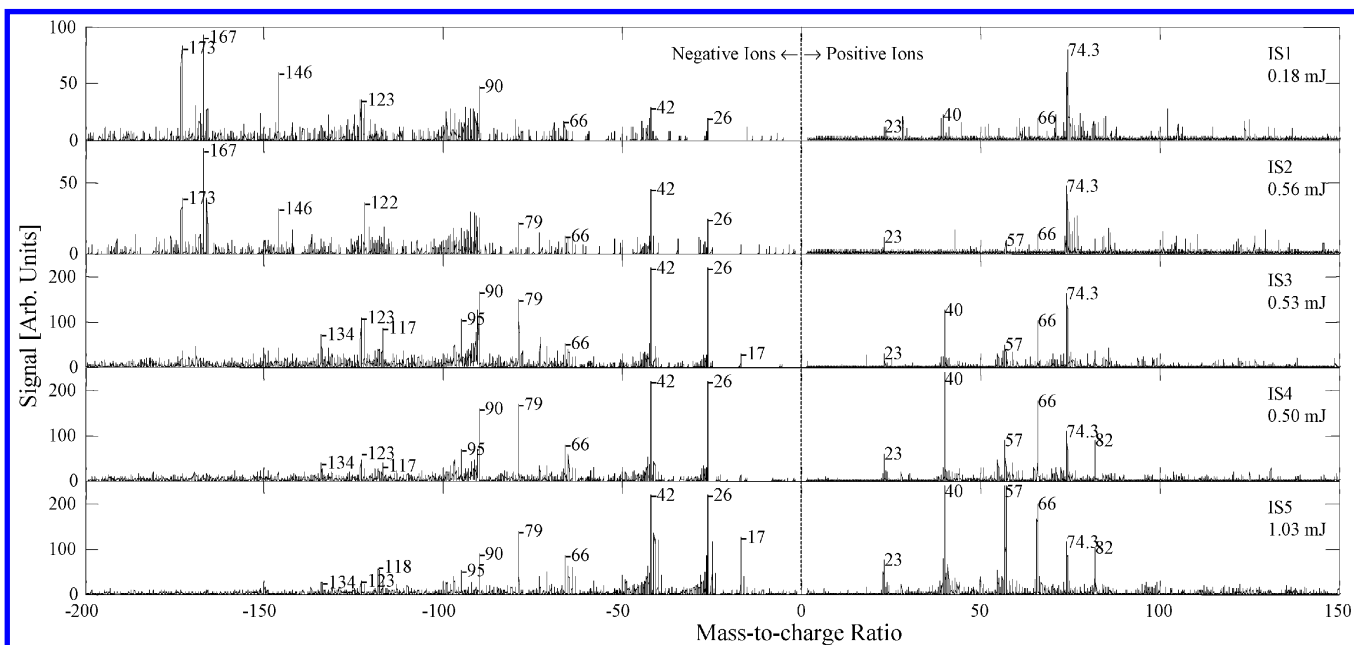


Figure 4. Individual spectra (IS) from single spores of *B. subtilis* var. *niger* collected with three different laser energy settings. The vertical scale is arbitrary but consistent from spectrum to spectrum in all figures. Although the three middle spectra are taken with the same approximate pulse energy, the first (IS2) resembles the low-energy spectrum (IS1), the last (IS4) resembles the high-energy spectrum (IS5), and the middle (IS3) resembles neither. We argue that the similar spectra may have been generated with similar fluences even though the total pulse energies were different.

represent the same number of ions). We believe that this is the first article to show both the positive and negative mass spectra generated from the same individual biological particle (regardless of how the spectra may be plotted).

The spectra IS1, IS3, and IS5 in Figure 4 are more or less typical of the spectra collected at the laser energies used to generate them (0.21, 0.50, and 1.02 mJ, respectively). Although the three middle spectra were taken with the same approximate pulse energy, the 0.56-mJ spectrum (IS2) resembles the 0.18-mJ spectrum (IS1), the 0.50-mJ spectrum (IS4) resembles the 1.03-mJ spectrum (IS5), and the 0.53-mJ spectrum (IS3) is unique. It is apparent that IS1, collected with the lowest pulse energy, has the most prominent "high-mass" peaks (defined here as  $|m/q| > 150$  for negative ions) and the least prominent low-mass peaks. IS5, collected with the highest pulse energy, has the least prominent high-mass peaks and the most prominent low-mass peaks. All of this can be consistently explained as a result of the laser profile once we demonstrate below that differences in absorbed energy produce these kinds of variations. Before we do that, however, we will first identify some of the ion peaks.

Most of the prominent peaks seen in the spectra shown in Figure 4 have been tentatively identified. The identifications are based on spectra acquired from DPA, DNA, and various amino acids as well as *Bacillus* grown in isotopically labeled growth media (an article detailing the experiments is in preparation). The peak at  $m/q = -173$  is ascribed to arginine. A metabolic precursor of DPA, 2,3-dihydrodipicolinate, was assigned to the peak at  $m/q = -169$ . The peaks at  $m/q = -167$ ,  $-166$ , and  $-122$  are believed to represent the molecular ion of DPA and two of its fragments. DPA is found almost solely in spore-forming bacteria so these peaks are particularly useful for identification purposes. Peaks at  $m/q = -146$  and  $-134$  are attributed to glutamic and aspartic acid, respectively. Glutamic acid in particular is known

to be common in *Bacillus* spores. Peaks at  $m/q = -97$  and  $-79$  are attributed to  $\text{H}_2\text{PO}_4^-$  and  $\text{PO}_3^-$  from phosphates found, for example, in nucleic acids and cell membranes. Peaks at  $m/q = -42$ ,  $-26$ , and  $+23$  are identified as  $\text{CNO}^-$ ,  $\text{CN}^-$ , and  $\text{Na}^+$ , respectively. The DPA in spores is usually associated with calcium. Peaks at  $m/q = +40$ ,  $+57$ ,  $+66$ , and  $+82$  are attributed to  $\text{Ca}^+$ ,  $\text{CaOH}^+$ ,  $\text{CaCN}^+$ , and  $\text{CaCNO}^+$ , respectively. The prominent peaks at  $m/q = -90$  and  $+74.3$  remain to be identified. (The mass of the latter peak was the only prominent peak mass to vary significantly from an integer mass-to-charge ratio, so an extra decimal value was kept.) Several of the peaks discussed here are similar to peaks that were identified in single-particle *B. subtilis* spectra obtained by Gieray et al.<sup>23</sup> That study, however, utilized significantly higher fluences ( $\sim 20 \text{ nJ}/\mu\text{m}^2$ ) at a different wavelength (308 nm), so it is not surprising that there are also clear differences between our spectra and theirs.

As explained earlier, profile variations produce variations in the energy absorbed by spores, but it remains to be proven that these absorbed energy variations actually have an effect on the mass spectra. Since the energy absorbed by a single spore cannot be determined, the average energy absorbed and the average spectrum produced by a collection of spores must be considered instead. Figure 5 shows averages of 1000 spectra collected at each of the six laser settings used. Variations due to factors other than the laser setting are averaged out and cannot account for differences between spectra (ignoring very small statistical fluctuations). Figure 3 shows that each laser energy setting produces a different average fluence. This means that spores must absorb different amounts of energy, on average, at each of the laser settings. Since the spectra in Figure 5 are clearly different, the energy absorbed by a spore must affect the spectrum that it produces. This proves that the laser profile will produce variations in the mass spectra.

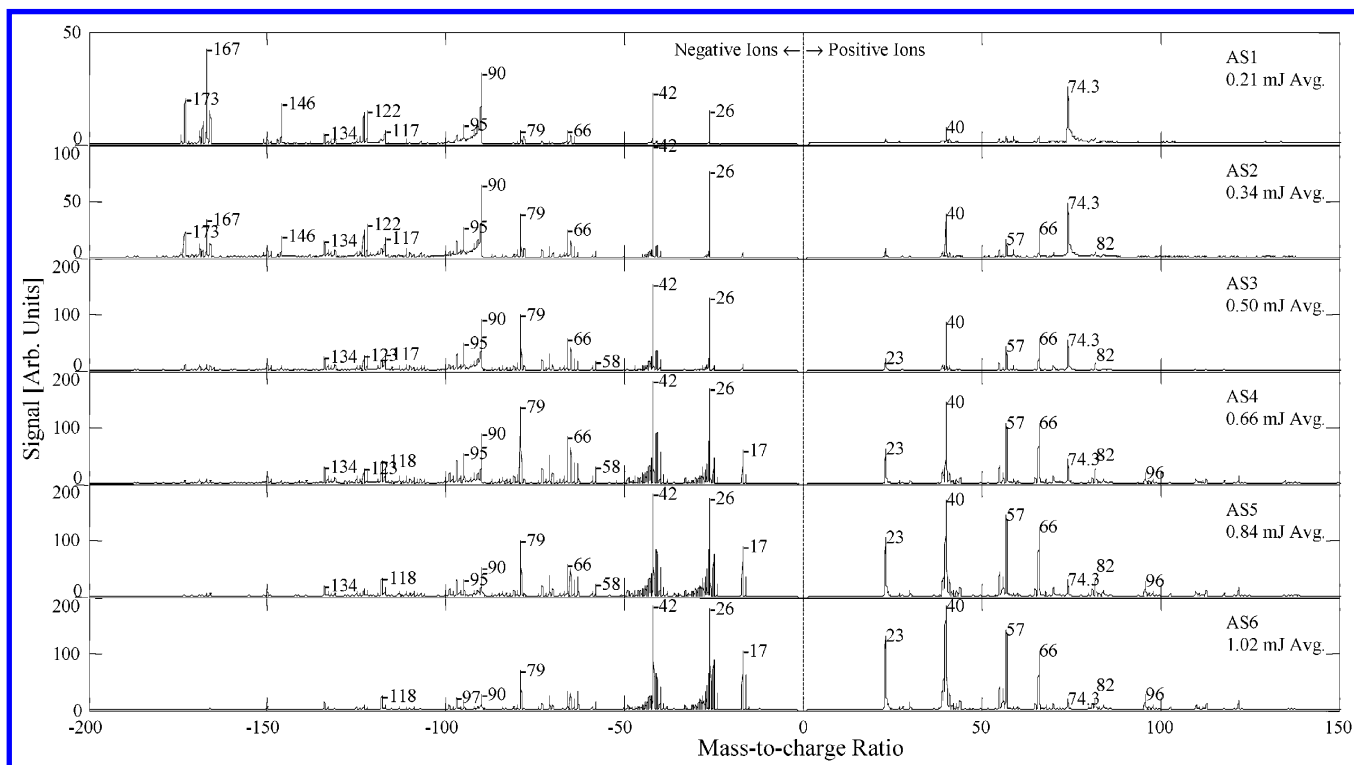


Figure 5. Averages of the 1000 spectra (AS) collected at each laser energy setting. The average pulse energy is labeled on each spectrum. The highest mass negative peaks are in AS1 and steadily decrease in AS2–AS6. The highest mass positive peaks, however, steadily increase and are greatest in AS6. The spectral differences result from changes in the average fluence produced by each laser setting. This leads us to conclude that the laser profile must introduce spectral variability from shot to shot since successive spores will interact with different regions (and different fluences) in the nonuniform profile and absorb different amounts of energy.

Before we further quantify the magnitude of the profile-induced variations, it is important to note the general trends in the average spectra of Figure 5. As the laser energy is increased, the amplitudes of high-mass negative peaks (in particular  $m/q = -173$  and  $-167$ ) are reduced and the negative low-mass peaks become more prominent. At low energy, the positive data are dominated by the peak at  $m/q = 74.3$ . As the pulse energy is increased, the peak initially grows and then declines. Most of the other peaks in the positive part of the spectrum grow monotonically with energy. In fact, the highest mass positive peaks are seen most clearly at the highest pulse energies (although they are much smaller than the low-mass positive peaks). The trends in the average spectra are consistent with the changes observed above between the individual spectra IS1, IS3, and IS5.

We have, so far, shown that profile-related fluence variations must produce variations in the mass spectra, but we have not indicated their magnitude. It is readily shown that the range of profile-induced spectral variations is at least as large as the difference between AS1 and AS6 (and could be even larger). Our line of reasoning is based on the hypothesis that spores that interact with the same fluence must, on average, produce the same mass spectra (even if the laser setting is changed or there are other sources of variability). From Figure 3 we know that the ranges of fluence produced by the six laser settings are broad and overlap significantly. Note in particular that the highest laser setting produces a range of fluences that covers and exceeds the range of fluences produced by the lower laser settings. If a large number of mass spectra were collected using the highest laser setting, it would be possible, in principle, to select a subset of the

spectra that were produced by the same distribution of fluences that led to AS1 and, therefore, when averaged would produce a spectrum identical to AS1. It would in fact be possible to reproduce any of the average spectra in Figure 5. Similarly, subsets of data collected at the second highest laser energy setting could reproduce spectra AS1 through AS5 and so on. Since averaged subsets of data can produce variations of this magnitude, the variations between individual spectra must be at least as great.

Finally, we will argue that natural variations (or other potential sources of variation) cannot be significantly larger than profile-induced variations. We will show that when similar spectra are grouped together, the resulting groups appear and behave as though the spectra in a given group were generated at a similar fluence level. If natural variations (or other random variations) were significantly larger than profile-induced variations, the spectra should not group together in this manner. We must admit, however, that these arguments are not entirely rigorous. Independent of our profile arguments, however, the clustering of similar spectra is important for automated identification algorithms so we feel that it merits discussion here.

The clustering algorithm employed is a modified ART2a neural network<sup>10</sup> that we have named bunched adaptive resonance theory. It will be described in more detail in a separate publication. Briefly, the automated grouping (clustering) of spectra into distinct groups of similar spectra is performed as follows. Each half of each spectrum is independently calibrated, and the locations and areas of ion peaks are determined. The peak information is then condensed into two 350-element vectors (one vector for positive ions and one for negative ions). The  $n$ th element of each vector

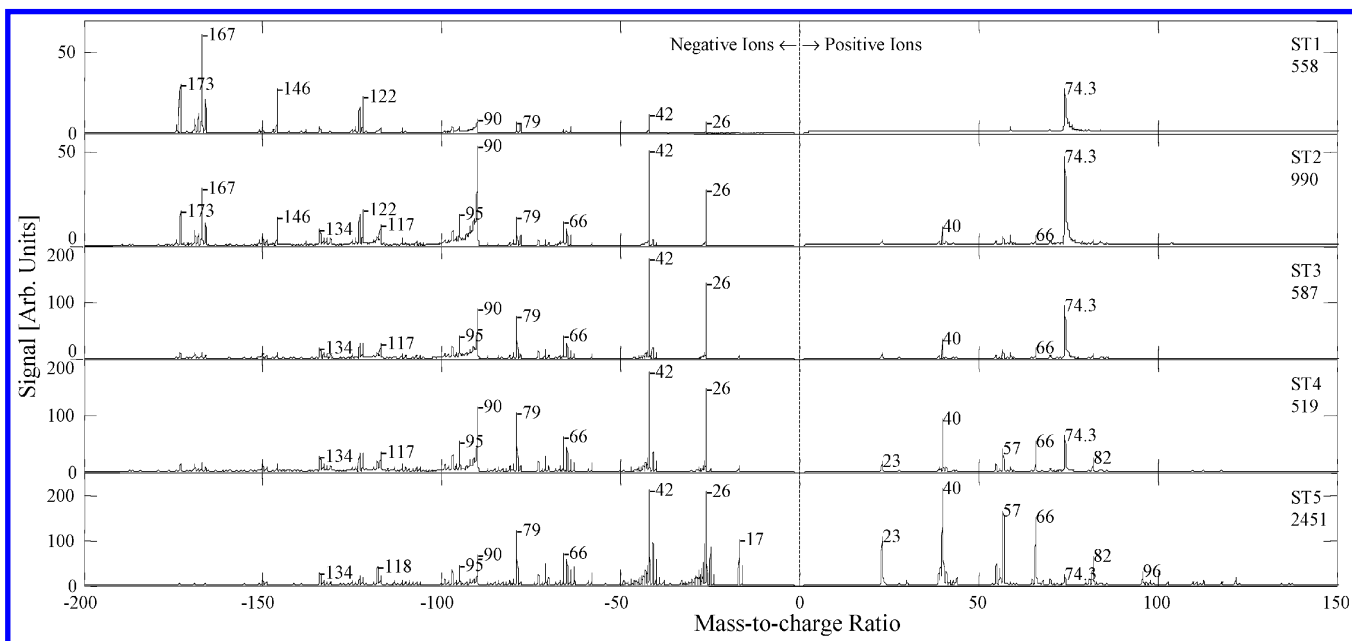


Figure 6. Averages from five clusters of spectra. Each cluster is a group of similar individual spectra and so its average spectrum can be thought of as a spectral type (ST). The spectral types are sorted by the average of the laser pulse energies measured for every laser shot used to generate the spectra in each cluster. This produces an arrangement that is clearly consistent with the power-dependent trends established in Figure 5. This in turn supports our belief that each spectral type is largely formed from spectra generated at a particular fluence. The number of spectra in each cluster is indicated below the spectral type label.

represents the integrated area of the ion peaks near the corresponding integer mass-to-charge ratio  $|m/q| = n$ , where  $n$  ranges from 1 to 350. Ion peaks with mass-to-charge ratios greater than 350 (which are rare) are ignored for the purposes of clustering. Once the half-spectra have been reduced to vector form, the angle between vectors from different particles can be calculated and used as a quantitative measure of their similarity. Similar spectra produce similar vectors separated by a small angle. Spectra that have no peaks in common produce orthogonal vectors. When the software compares spectra from two aerosol particles, the angle between the positive ion vectors is calculated and then the angle between the negative ion vectors is calculated. If both angles are less than a specified value, the particles are considered a match and are put into a single cluster.

The data collected at all six laser energy settings were combined and then processed with our software. This resulted in a total of five clusters of spectra containing 5105 of the initial 6000 spectra (85%). The 895 spectra that were excluded had atypical features resulting, for example, from calibration errors (introduced by the automated calibration routine), impurities in the spore solution, or fragmented spores. The individual spectra in each cluster were averaged to obtain the spectra shown in Figure 6. Since individual spectra are only averaged with similar individual spectra, Figure 6 presents a better picture of the range of variability in the data than Figure 5 (where very different spectra were averaged together because they were produced at the same laser setting). It is appropriate, therefore, to treat the average cluster spectra as "spectral types". This is important because an automated identification routine that compares an unknown spectrum to previously determined spectral types would be more likely to find a close match than another routine that compares an unknown spectrum with averages like those in Figure 5.

If most spectral variability truly resulted from fluence variations in the laser profile, the spectra that happened to be generated at a fixed fluence would show little variability and should cluster together (i.e., each spectral type would represent a specific range of fluences). Spectral types that represent high fluences would be composed largely of spectra collected with high laser pulse energies (since these pulses contain the most area at high fluence). Clusters that represent low fluences would be composed largely of spectra collected with low laser energies. The averages of the laser pulse energies individually measured for every spectrum in each cluster would, therefore, provide some indication of the fluence level represented by each spectral type. These average energies were calculated, and the spectral types in Figure 6 are presented in order of this value. ST1 has the lowest average pulse energy while ST5 has the highest. It is reassuring, therefore, that the progression of spectral types is consistent with the power-dependent trends identified in Figure 5. ST1 clearly looks like it is generated at the lowest fluence, ST2 at a slightly higher fluence, and so on.

Figure 7 shows the distribution of spectral types collected at each laser setting. In general, the trends in the data are consistent with the expected power-dependent behavior. The "low-fluence" spectral types are primarily produced with low pulse energies and the "high-fluence" spectral types are primarily produced with high pulse energies. An important observation is that spectra of all spectral types are produced at all laser energy settings, just at different ratios. This implies that all of the spectral types can be produced with fluences below  $\sim 2 \text{ nJ}/\mu\text{m}^2$  since the lowest energy pulses contain almost no area at a greater fluence. Fluences much above  $2 \text{ nJ}/\mu\text{m}^2$  evidently produce spectra that generally fall into spectral type 5 (ST5). The fact that ST5 has nearly two and a half times as many members as any of the other types is consistent

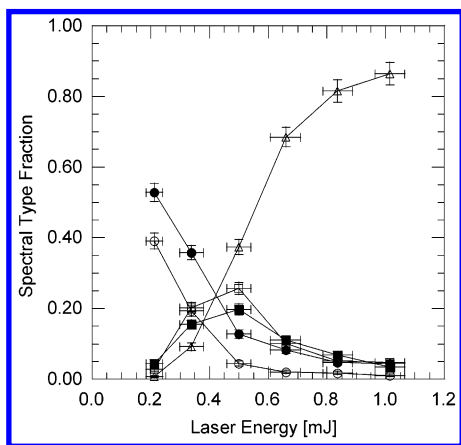


Figure 7. Relationship between spectral type and laser energy. Spectral types believed to represent low-fluence spectra (ST1 ○ and ST2 ●) are produced primarily from low-energy pulses. ST3 (□) and ST4 (■) appear to represent higher fluences and are largely produced by higher energy pulses. The highest energy pulses, however, overwhelmingly produce spectral type ST5 (△). Nonetheless, it is important to note that all of the spectral types are produced at all of the laser energy settings.

therefore with the fact that most of the area in the profiles is well above  $2 \text{ nJ}/\mu\text{m}^2$ . It is difficult to explain how natural variations (or other sources of variability) would produce this type of behavior. It appears that natural variations cannot be significantly more important than the profile induced spectral variations.

Before concluding, we note that all spectral types, ST1–ST5, are characteristic of bacterial spores and are distinct from many other aerosols as will be shown in a separate publication.<sup>25</sup> All of the spectral types have value for identification purposes, but ST1 and ST2 are preferred because of their more prominent high-mass peaks (e.g., those indicative of DPA). Figure 7 could easily be interpreted, therefore, as implying that the lowest laser energy is optimal since it produces the largest fraction of these two spectral types. The hit rate, however, is an important and practical factor that must also be considered; not every particle that is fired upon by the D/I laser produces a spectrum. Figure 8 shows the number of type ST1 and ST2 spectra obtained divided by the number of D/I laser shots fired versus laser energy. The rate at which the laser fires is roughly constant; thus, the ratio is approximately equivalent to the rate (in time) at which “good” spectra are acquired and can be considered a figure of merit. The plot in Figure 8 reveals that the second lowest pulse energy (0.33 mJ) is in fact optimal in this sense. Of course it is not the pulse energy itself that is of ultimate importance. Rather it is the fluences produced and the areas over which they are spread.

## CONCLUSIONS

We have found that a nonuniform D/I laser profile causes significant variability in the spectra generated from single *Bacillus*

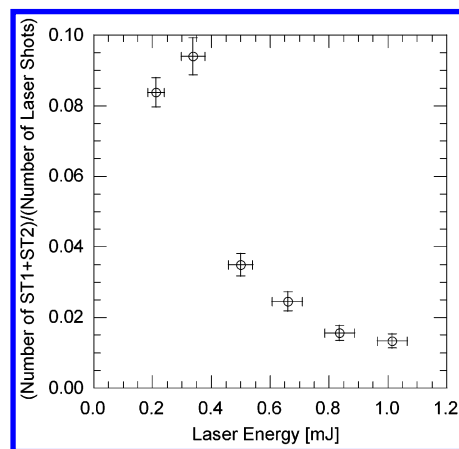


Figure 8. Spectral types ST1 and ST2, which contain prominent peaks at  $m/q = -167$  and  $-173$ , are believed to be particularly useful for identification purposes. Figure 7 shows that the lowest laser energy (0.21 mJ) produces the greatest fraction of ST1 and ST2, but this does not take into account the rate at which spectra are produced. When the number of laser shots required to produce the “good spectra” is factored in, the laser setting of 0.33 mJ/pulse is found to be optimal. This optimal setting produces the greatest number of good spectra in a fixed amount of time and therefore helps maximize the sensitivity of the BAMS system.

spores. This variability is clearly undesirable in BAMS or any other system that must identify single-particle mass spectra with high confidence. Most single-particle mass spectrometers used today employ lasers with profiles similar to ours, so we believe that this is an important observation. In some applications, the identification of spectral types may help deal with the resulting spectral variability, but generally it seems preferable to simply reduce the variability directly. Whatever natural particle variations may be present cannot be eliminated, but the laser profile can be improved. In the case of BAMS, this work is in progress as are experiments with other wavelengths, pulse lengths, and different threat agent simulants.

## ACKNOWLEDGMENT

This work was performed under the auspices of the U.S. Department of Energy by University of California Lawrence Livermore National Laboratory under Contract W-7405-ENG-48. This work is supported by the Lawrence Livermore National Laboratory through Laboratory Directed Research and Development Grant 02-ERD-002. This project was funded in part by the Technical Support Working Group of the Department of Defense.

Received for review April 22, 2003. Accepted August 5, 2003.

AC034419U